Journal of Organometallic Chemistry 903 (2019) 120981

Contents lists available at ScienceDirect

Journal of Organometallic Chemistry

journal homepage: www.elsevier.com/locate/jorganchem

Mechanism and stereospecificity of Z-enamide synthesis from salicylaldehydes with isoxazoles using DFT calculations

Baoping Ling [a, b, *], Yuan-Ye Jiang [b], Yuxia Liu [b], Peng Liu [b], Rutao Liu [a, **], Siwei Bi [b, ***]

[a] School of Chemistry and Chemical Engineering & School of Environmental Science and Engineering, Shandong University, Jinan, Shandong, 250100, China
[b] School of Chemistry and Chemical Engineering, Qufu Normal University, Qufu, Shandong, 273165, China

ARTICLE INFO

Article history:
Received 26 July 2019
Received in revised form
1 October 2019
Accepted 13 October 2019
Available online 17 October 2019

Keywords:
Z-enamides
Salicylaldehyde
Isoxazole
DFT calclulations
Stereospecificity
Catalytic mechanism

ABSTRACT

A mechanistic study on Rh-catalyzed synthesis of stereospecific Z-enamide from salicyladehydes and isoxazoles has been performed with DFT calculations. The aldehydic C–H bond activation was found directed by anionic phenolic group rather than neutral phenolic hydroxyl, which reasonably rationalizes the reversibility of the C–H bond activation. Direct ring-opening rather than N–O oxidative addition of isoxazole, and subsequent C–C reductive elimination generate the stable tripodal intermediate that has been demonstrated by LC-MS analysis. Finally, sequential amino and phenolic protonations of the tripodal species produce the product Z-enamide. Stereospecificity of Z-enamide can be attributed to the rigid carbon-carbon double bond formed by direct ringopening of isoxazole. The rate-determining process is found to include the directing ring-opening and C–N reductive elimination with an overall barrier of 26.7 kcal/mol.

1. Introduction

The enamides have attracted much interest in organic synthesis [1], and have been found broad applications in bioactive natural product and pharmacological field as nucleophilic synthons [2]. In recent years, the enamides have been widely used as the powerful intermediates to synthesize the heterocycles [3] due to their enhanced stability. In particular, the second enamides have exhibited reactive behavior towards highly electron-deficient unsaturated reactants [4]. The synthetic methods of enamides involve the reaction of ketone with the second amine [5], the reductive reaction of ynamine [6], and Curtius rearrangement [7]. Various transition-metal catalysts, such as copper, iridium, palladium and ruthenium, have been applied in the transposition of the terminal C=C of the corresponding allylamides to achieve a wide range of enamides [8]. Usually, these methods thermodynamically favor the E-configured enamides or lead to the Z/E mixture, and failed to provide a synthetic route to obtain the stereospecific Z-configured enamide.

Recently, Maji and coworkers [9] presented an advanced strategy for the stereospecific synthesis of Z-enamides. They used isoxazole as a masked electrophile in C–H functionalization of salicyladehyde to afford the desired stereospecific formation of Z-enamide (Scheme 1). They disclosed a novel approach for the synthesis of Z-enamides with an exclusive Z-selectivity, a benign reaction condition and considerable yields. In previous experimental studies, some literatures presented that the phenolic group in salicylaldehyde coordinates with Rh center as an anionic ligand [10], but some proposed that it does as a neutral ligand [11]. However, the theoretical reports about the coordination mode of the phenolic group in salicylaldehyde to the transition metal center are rare, thus its coordination mode is still unclear. In this work, some key issues were further explored with DFT calculations, (1) coordination mode of the phenolic group of salicylaldehyde, a neutral ligand or an anionic ligand? (2) origin of the stereospecificity of enamides? (3) N–O bond cleavage mode.

2. Computational details

All density functional theory (DFT) calculations were performed

* Corresponding author. School of Chemistry and Chemical Engineering & School of Environmental Science and Engineering, Shandong University, Jinan, Shandong, 250100, China.
** Corresponding author.
*** Corresponding author.
E-mail addresses: xiaoling0523@163.com (B. Ling), rutaoliu@sdu.edu.cn (R. Liu), siweibi@126.com (S. Bi).

https://doi.org/10.1016/j.jorganchem.2019.120981
0022-328X/

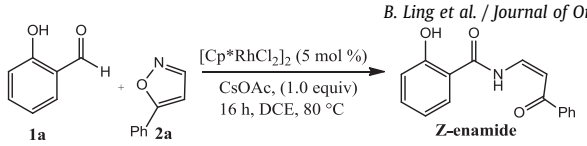

Scheme 1. Title Reaction.

by using Gaussian 09 program [12]. Molecular geometries of all the intermediates and transition states were optimized at the M06 level of theory [13] in conjugation with the ultrafine grid [14]. The effective core potentials of Hay and Wadt with a double-ζ basis set (LANL2DZ) [15] were used for Rh ($\zeta_f = 1.350$), and the 6-31G(d,p) basis set [16] was used for C, O, N and H atoms (BS1). Vibration frequency calculations were conducted at the same level to confirm the optimized structures as minima (no imaginary frequency) and transition states (no imaginary frequency), and to obtain the thermodynamic corrections. All transition -state structures were verified to connect two relevant minima by using intrinsic reaction coordinate (IRC) calculations [17].

The solvent effect was treated with a self-consistent reaction field (SCRF) using the SMD model [18]. The energies were refined by single-point calculations using the larger basis set 6-311++G(d,p) for C, O, N and H atoms and SDD for Rh (BS2). Dichloroethane (DCE) was used as the solvent with a dielectric constant value of 10.125. Additional density functionals such as B3LYP [19], M06L [20] and ωB97XD [21] were applied for the key intermediates and transition states, and the calculated results show the similar trend with M06/6-311++G(d,p) (Table S1). Unless specifically mentioned, all the energies discussed throughout the main text were the solution-phase relative free energies corrected at 298 K and 1 atm in gas phase.

3. Results and discussion

A plausible catalytic cycle (Scheme 1) was proposed by Maji et al. [9]. The active catalyst **A** undergoes C–H metalation with salicylaldehyde **1a** to generate a five-membered rhodacycle **B**, which is coordinated by **2a** to give intermediate **C**. A N–O bond cleavage takes place to afford a nitrido intermediate **D**, which experiences migration/insertion of nitrene into the Rh–C bond to deliver a tripodal intermediate **7**. Finally, protonolysis of intermediate **7** produces the desired Z-enamide **3a** and regenerates the catalyst. On the basis of plausible mechanism, the detailed DFT calculations were performed.

3.1. Formation mechanism of the five-membered rhodacycle intermediate

[Cp*Rh(OAc)$_2$] (**Cat**) formed in the reaction system was chosen as the initial active catalyst (Fig. S1). To clarify the coordination mode of phenolic group in salicylaldehyde, two plausible modes were considered. Maji et al. proposed that salicylaldehyde **1a** undergoes C–H metalation catalyzed by the active catalyst [Cp*Rh(OAc)$_2$] to give a five-membered rhodacycle intermediate via a direct C–H functionalization (Scheme 2) [9–11]. Based on the proposal, the direct C–H activation of **1a** was calculated with the phenolic group of salicylaldehyde coordinated to Rh as a neutral ligand, as shown in Fig. 1. However, this step can be ruled out because the overall energy barrier is extremely high, 51.0 kcal/mol. Coordination of **1a** to Rh center as a neutral ligand forms intermediate **IM1′** that undergoes a direct C–H metalation to yield intermediate **IM2′** via an unstable transition state **TS1'**. The infeasibility of such a C–H activation step is resulted from the unreasonable transformation from **IM1'** (18e) to **IM2'** (20e). To further verify whether the phenolic group of salicylaldehyde could serve as

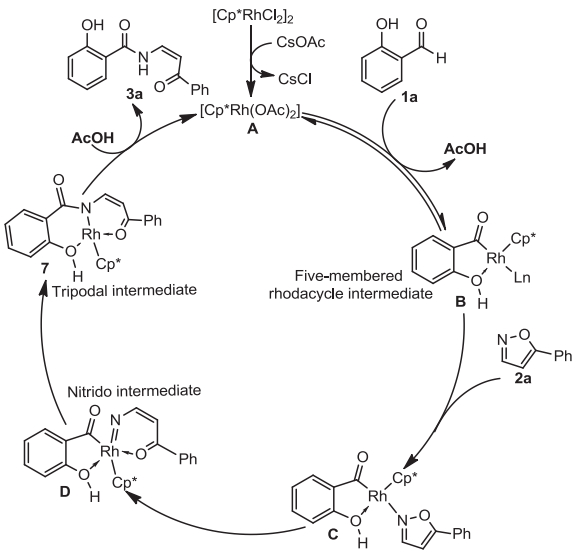

Scheme 2. Plausible Mechanism proposed by Maji et al.

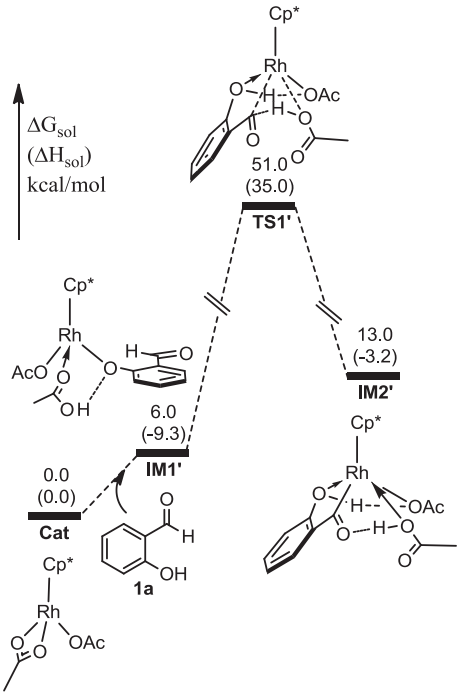

Fig. 1. Gibbs free energy profile for the C–H metalation of salicylaldehyde with phenolic group as a neutral ligand.

a neutral ligand, we calculated the ensuing step for the N–O bond cleavage of isoxazole. The direct ring-opening of isoxazole is also inaccessible because this step requires an overall energy barrier of 34.6 kcal/mol (Fig. S2A). Our attempts to locate another intermediate with different regioselectivity of isoxazole for the direct ring-opening have failed. In addition, the oxidative addition for the N–O bond cleavage was also considered, but this step can be ruled out owing to the extremely high activation barriers of 55.0 and 55.8 kcal/mol (Figs. S2B and S2C). Therefore, these results indicate that the phenolic group of salicylaldehyde coordinating to Rh as a neutral ligand is unfavorable in the Z-enamide synthesis with isoxazoles.

An alternative coordination mode [10] that the phenol group acting as an anionic ligand was also considered. The detailed C–H activation process is given in Fig. 2. As shown in Figure 2, **1a** binds to **Cat** through the hydrogen bond to form intermediate **IM1**, which then undergoes ligand exchange with **1a** to afford **IM2** via **TS1-2**, and this step overcomes the overall energy barrier of 10.2 kcal/mol. Deprotonation of phenol group in salicylaldehyde takes place to give **IM5** via a concerted metalation-deprotonation (CMD) [14(d) [22]] process (**IM3**→**IM5**), and this step is easy to occur with a barrierless process. After release of acetic acid, the C–H activation via CMD process (**IM6**→**IM8**) requires the overall energy barrier of 17.7 kcal/mol, and it is exergonic by −7.0 kcal/mol to yield **IM8**. Then, another acetic acid is released from **IM8** to generate a five-membered rhodacycle intermediate **IM9**. It is noted that the overall energy barrier for the reverse reaction (**IM8**→**IM6**) is calculated to be 24.7 kcal/mol, thus, the reversibility of the C–H activation is feasible in the absence of **2a** at the experimental temperature (80 °C), which is supported by the sufficient C–H/D exchange experiment [9]. Therefore, the C–H activation of salicylaldehyde is facile to occur and reversible, which can be rationalized through the mechanism with phenolic group as an anionic ligand. In addition, we have also considered a cation pathway as shown in Fig. S3, in which the catalyst reacts with **1a** to produce a cation to initiate the reaction, but the Gibbs free energy of 25.2 kcal/mol is thermodynamically unfavorable for the reaction.

3.2. Formation mechanism of the tripodal intermediate

Starting from **IM9**, the isoxazole coordinates to Rh center to give two intermediates with isoxazole having opposite orientations (**IM10** and **IM10′**) as shown in Fig. 3, both of which are energetically similar with relative free energies of −9.0 and −9.3 kcal/mol. **IM10** undergoes a direct ring-opening process via **TS11** to yield a nitrido intermediate **IM12** with a barrier of 20.7 kcal/mol. Subsequently, the N–C bond reductive elimination from Rh occurs to give a tripodal intermediate **IM14** via **TS13** with an overall barrier of 26.7 kcal/mol (**TS13** → **IM10**). This process is significantly exergonic by 46.0 kcal/mol as a result of the C–N and CO→Rh bond formation. The sharp signal found at *m*/*z* 504.3 in LC-MS spectra suggests the formation of the tripodal intermediate [9], which was supported by the computed stable tripodal intermediate **IM14**. Similarly, **IM10′** also undergoes direct ring opening and C–N reductive elimination to finally give **IM14-c**. It can be seen that **TS13-c** is 1.5 kcal/mol above **TS13**, suggesting both pathways are competitive with the black pathway slightly favorable. **IM14-c** is

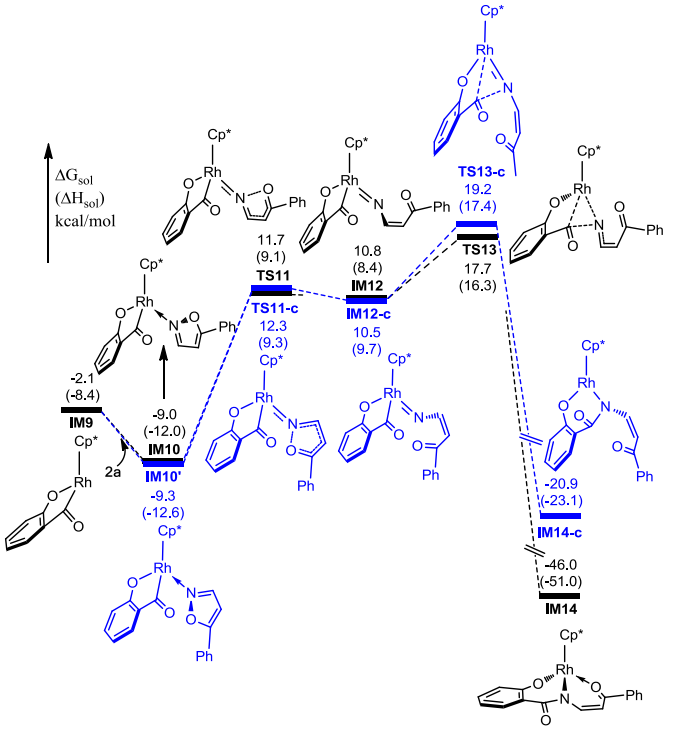

Fig. 3. Gibbs free energy profile for the direct N–O bond cleavage and C–N reductive elimination process.

less stable than **IM14** due to the lack of CO→Rh bond. It is noted that a rigid C=C double bond formation from direct ring opening of isoxazole retains the stereospecicifity of Z-enamide.

As mentioned above, the N–O bond cleavage is achieved by direct ring opening. An alternative N–O bond cleavage by oxidative addition to Rh(III) was also considered herein. As shown in Fig. 4, the barriers to N–O oxidative addition from **IM10** and **IM10'** were calculated as high as 41.1 and 42.5 kcal/mol, respectively. The difference between the direct ring opening and oxidative addition pathways can be clarified using distortion interaction analysis [23], which is also known as the activation strain model [24]. Fig. 5 presents the relationship among $\mathbf{A_0}$ and $\mathbf{B_0}$ obtained by optimization, fragments **A** and **B** obtained directly derived from **TS11** and **TS11-a**. ΔE_1, $\Delta E_1^{'}$, ΔE_2 and $\Delta E_2^{'}$ represent distortion energies, while

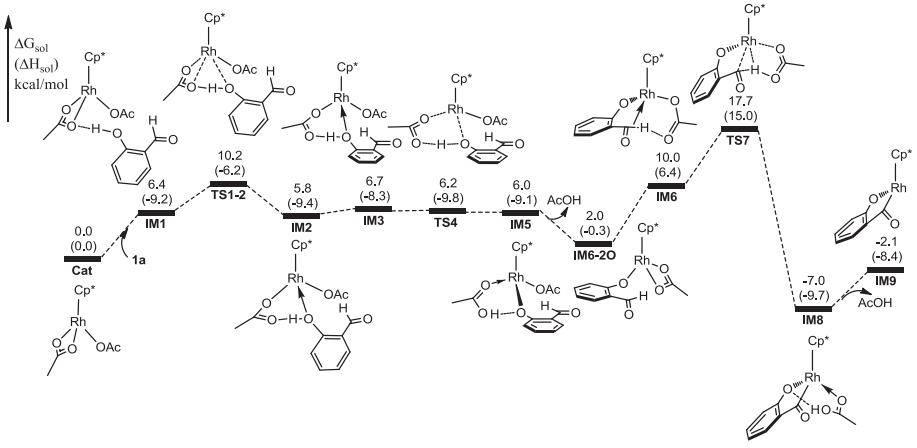

Fig. 2. Gibbs free energy profile for O–H deprotonation and C–H metalation process.

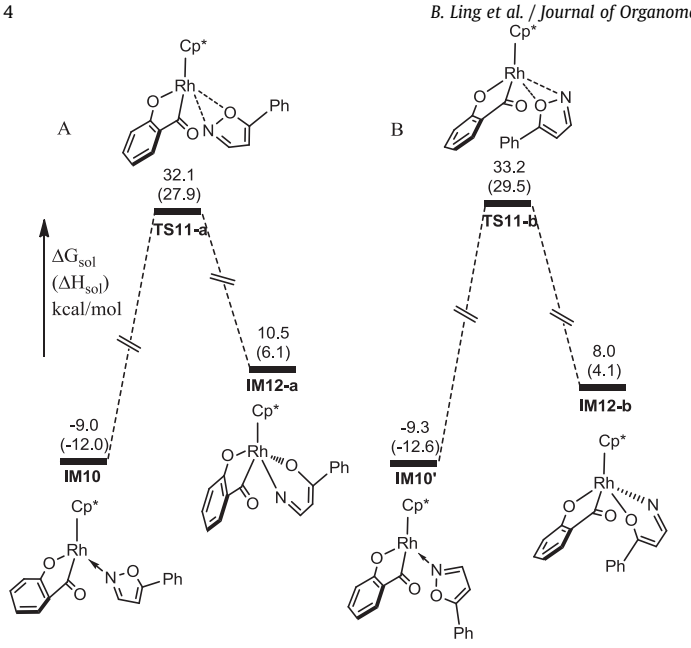

Fig. 4. Gibbs free energy profiles for N—O oxidative addition of isoxazole with phenolic group as an anionic ligand.

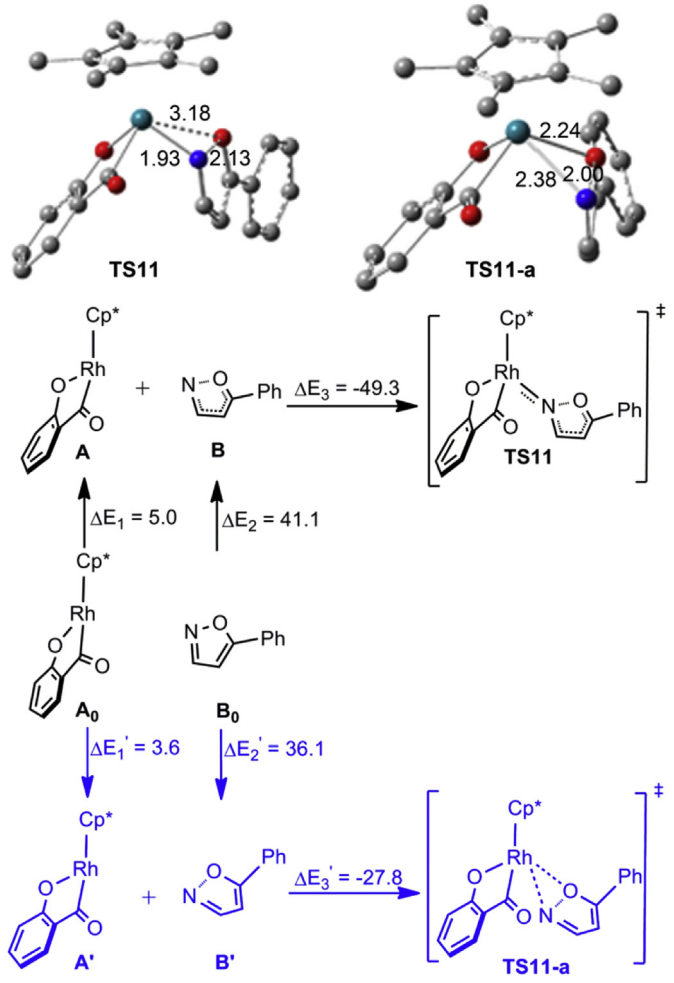

Fig. 5. Distortion interaction analysis for **TS11** and **TS11-a**.

ΔE_3 and $\Delta E_3^{'}$ represent interaction energies. ΔE_1 and $\Delta E_1^{'}$ are close in energy indicating the rhodacyclic fragment undergoes a small distortion and contributes little to the energy difference of **TS11** and **TS11-a**. ΔE_2 and $\Delta E_2^{'}$ have an energy difference of 5.0 kcal/mol, contributing a little to the energy difference of **TS11** and **TS11-a**. The higher distortion from $\mathbf{B_0}$ to **B** arises from the longer N—O distance (2.13 Å) compared to the one in **B'** (2.00 Å). More importantly, the interaction energies of ΔE_3 and $\Delta E_3^{'}$ have an energy difference of 21.5 kcal/mol. Consequently, the big difference in interaction energy is the major reason leading to both transition states having different stabilities. Examining the geometries of **TS11** and **TS11-a**, one can see the Rh—N bond (1.93 Å) in the former is obviously shorter than the Rh—O bond (2.24 Å) in the latter, indicating the stronger Rh—N interaction provides major contribution to the interaction energy ΔE_3. In conclusion, stronger N—Rh interaction leads to **TS11** more stable.

3.3. Proteolysis of tripodal intermediate and the catalyst regeneration

Fig. 6 shows the energy profile for the product release and the catalyst regeneration. From **IM14**, the sequential amino and oxygen protonations occur to afford the Z-enamide and regenerate the catalyst. First, coordination of acetic acid to Rh center together with a N···H—O hydrogen bonding leads to dissociation of the carbonyl to deliver **IM15**. Then, the amino protonation (**IM15**→**IM17**) takes place easily. One more acetic acid again coordinates to Rh center to protonate the oxygen atom with a barrierless process (**IM18**→**IM20**). Finally, Z-enamide is released from the Rh center and the catalyst is regenerated. This process needs to overcome an overall free energy barrier of 21.8 kcal/mol, which is lower than that for formation of the tripodal intermediate. Although the relative free energy of product **P** is slightly higher than that of **IM14** by 1.8 kcal/mol, which seems to be unfavorable thermodynamically, but this case is feasible for catalytic reactions [25].

Starting from **IM14**, we have also considered the alternative pathway with a reversed sequence, *i.e.*, oxygen-protonation prior to amino-protonation, and the corresponding energy profile is given in Fig. S4. This process is disfavored due to the high energy barrier of 37.3 kcal/mol (**IM14**→**TS19′**). In addition, the protonolysis of competitive intermediate **IM14-c** has also been considered, and the detailed energy profile is shown in Fig. S5. The pathway from **IM15-c1**→**P**, amino-protonation prior to oxygen-protonation, is more favorable with the lower energy barrier of 10.9 kcal/mol.

In summary, the complete catalytic cycle for the Z-enamide synthesis from salicylaldehyde coupling with isoxazole has been improved and as shown in Scheme 3. The salicylaldehyde **1a** as an anion ligand coordinates to the active catalyst [Cp*Rh(OAc)$_2$] through the O—H deprotonation, undergoing C—H metalation to afford a five-membered rhodacycle intermediate **IM9**. The isoxazole **2a** coordinates with Rh center to give **IM10** with the nitrogen atom closing to the carbonyl of salicylaldehyde for the convenience of C—N reductive elimination. Then, the direct ring-opening of isoxazole takes place to generate the nitrido intermediate **IM12**, which experiments the C—N reductive elimination to deliver a tripodal intermediate **IM14**. This is consistent with the experimental result that the tripodal intermediate **IM14** has been demonstrated by LC-MS analysis. Finally, the sequential protonolysis of the amino group and oxygen atom by acetic acid occur to regenerate the catalyst and offer the desired Z-enamide. For the entire catalytic cycle, the process (**IM10**→**IM14**) involving direct ring opening of isoxazole and C—N reductive elimination is the rate-determining step with an overall energy barrier of 26.7 kcal/mol.

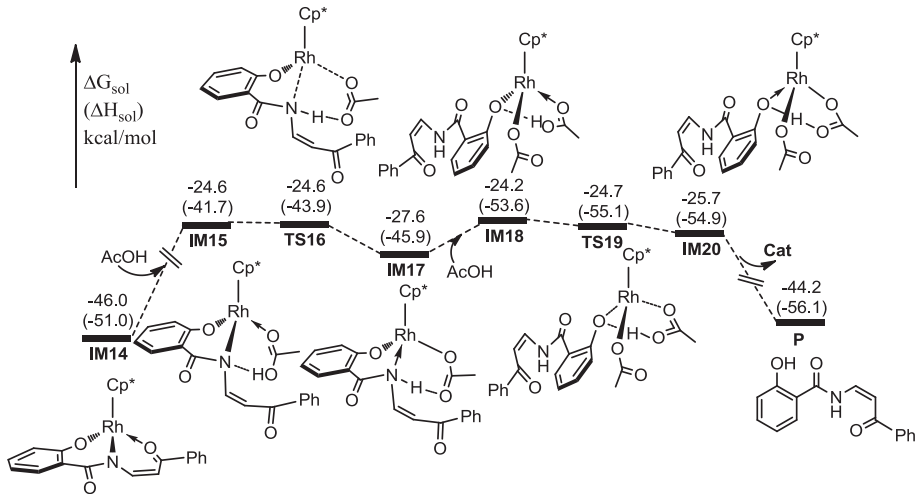

Fig. 6. Gibbs free energy profile for the protonolysis of tripodal intermediate and the catalyst regeneration.

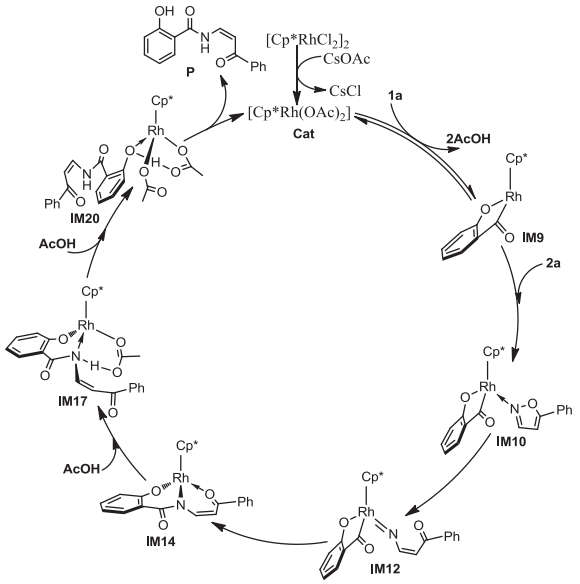

Scheme 3. Modified mechanism for the Z-enamide synthesis from salicylaldehyde and isoxazole.

4. Conclusions

A detailed computational study on the Rh(III)-catalyzed reaction of salicylaldehyde with isoxazole has been conducted, and an improved catalytic cycle has been presented. This mechanism involves sequential O—H deprotonation, aldehydic C—H metalation of salicylaldehyde, direct ring-opening of isoxazole, N—C reductive elimination, and protonolysis of amino and phenolic groups, generating the desired Z-enamide product. Major findings are found as follows. 1) The deprotonated anionic phenolic group rather than the neutral phenolic hydroxyl of salicylaldehyde acts as the directing group. 2) N—O bond cleavage of isoxazole occurs via a direct ring-opening rather than via N—O oxidative addition to Rh(III). 3) Direct ring-opening of isoxazole results in a rigid carbon-carbon double bond that enables stereospecific generation of Z-enamide. 4) The rate-determining process including direct ring opening (**IM10**→**IM12**) and C—N reductive elimination (**IM12**→**IM14**) with an overall activation barrier of 26.7 kcal/mol 5) The reversibility of aldehydic C—H bond activation can be rationalized based on our calculation results shown in Fig. 2.

Declaration of competing interest

The authors declare that they have no known competing financial interestsor personal relationships that could have appeared to influence the work reported in this paper.

Acknowledgement

This work was supported by the National Natural Science Foundation of China (Nos. 21603116, 21873055 and 21702119), Natural Science Foundation of Shandong Province (No. ZR2017QB001 and ZR2019MB016), and High Performance Computing Center of Qufu Normal University.

Appendix A. Supplementary data

Supplementary data to this article can be found online at https://doi.org/10.1016/j.jorganchem.2019.120981.

References

[1] (For selected examples of enamides): (a) F. Weber, P.S. Steinlandt, M. Ballmann, G. Hilt, Structure-dependent Nickel-Catalysed Transposition of N-Allyl-Amides to E- or Z-Enamides, Synthesis, vol. 48, 2016 (A-K);
(b) P. Caramenti, N. Declas, R. Tessier, M.D. Wodrich, J. Waser, Steroselective synthesis of alkyl-, aryl-, vinyl- and alkynyl-substituted Z-enamides and enol ethers, Chem. Sci. 10 (2019) 3223—3230;
(c) F. Beltran, L. Miesch, Tertiary enamide-triggered S_EAr: domino allylation and enamine-type addition, Org. Lett. 21 (2019) 1569—1573;
(d) X. Cai, M. Yang, H. Guo, Tertiary enamides: versatile and available substrates in synthetic chemistry, Curr. Org. Synth. 16 (2019) 70—97;
(e) A.R. Aguiar, E.S. Alvarenga, R.P. Oliveira, V.M.T. Carneiro, L.G. Moura, Syntheses of epoxides, and structural analysis of (E)-N-hexyl-3-(trans-3-methyloxiran-2-yl)prop-2-enamide by spectroscopic techniques and DFT, J. Mol. Struct. 1165 (2018) 312—317.
[2] (For selected examples, see): (a) M.J. Martín, L. Coello, R. Fernández, F. Reyes, A. Rodríguez, C. Murcia, M. Garranzo, C. Mateo, F. Sánchez-Sancho, S. Bueno, C. de Eguilior, A. Francesch, S. Munt, C. Cuevas, Isolation and first total synthesis of PM050489 and PM060184, two new marine acticancer compounds, J. Am. Chem. Soc. 135 (2013) 10164—10171;
(b) D. Prabhakar Reddy, N. Zhang, Z. Yu, Z. Wang, Y. He, Total synthesis of kanamienamide, J. Org. Chem. 82 (2017) 11262—11268.
[3] (a) M.-N. Zhao, Z.-H. Ren, D.-S. Yang, Z.-H. Guan, Iron-catalyzed radical cycloaddition of 2-H-azirines and enamides for the synthesis of pyrroles, Org. Lett. 20 (2018) 1287—1290;
(b) S.V. Kumar, A. Acharya, H. Ila, Synthesis of 2,4,5-trisubstituted oxazoles with complementary regioselectivity from α-oxoketene dithioacetals and β-

(methylthio)-β-(het)aryl-2-propenones, J. Org. Chem. 83 (2018) 6607–6622;
(c) W. Zhu, S. Tong, J. Zhu, M.-X. Wang, Intramolecular arylation of tertiary enamides through $Pd(OAc)_2$-catalyzed dehydrogenative cross-coupling reaction: construction of fused N-heterocyclic scaffolds and synthesis of isoindolobenzazepine alkaloids, J. Org. Chem. 84 (2019) 2870–2878.

[4] (For selected examples, see): (a) R. Matsubara, S. Kobayashi, Enamides and enecarbamates as nucleophiles in stereoselective C-C and C-N bond-forming reactions, Acc. Chem. Res. 41 (2008) 292–301;
(b) G. Dagousset, J. Zhu, G. Masson, Chiral phosphoric acid-catalyzed enantioselective three-component povarov reaction using enecarbamates as dienophiles: highly diastereo- and enantioselective synthesis of substituted 4-aminotetrahydroquinolines, J. Am. Chem. Soc. 133 (2011) 14804–14813;
(c) M. Terada, K. Machioka, K. Sorimachi, High substrate/catalyst organocatalysis by a chiral Brønsted acid for an enantioselectivity aza-ene-type reaction, Angew. Chem. Int. Ed. 45 (2006) 2254–2257;
(d) G. Bernadat, G. Masson, Enamide Derivatives: Versatile Building Blocks for Highly Functionalized α,β-Substituted Amines, Synlett., 2014, pp. 2842–2867.

[5] (a) J.A. Lutz, V.S. Don, R. Kumar, C.M. Taylor, Influence of sulfur on acid-mediated enamide formation, Org. Lett. 19 (2017) 5146–5149;
(b) P. Dupau, P. Le Gendre, C. Bruneau, P.H. Dixneuf, Optically active amine derivatives: ruthenium-catalyzed enantioselective hydrogen of enamides, Synlett (1999) 1832–1834.

[6] (For selected examples, see): (a) X. Zhang, Y. Zhang, J. Huang, R.P. Hsung, K.C.M. Kurtz, J. Oppenheimer, M.E. Petersen, I.K. Sagamanova, L. Shen, M.R. Tracey, Copper(II)-Catalyzed amidations of alkynyl bromides as a general synthesis of ynamides and Z-enamides. An intramolecular amidation for the synthesis of macrocyclic ynamides, J. Org. Chem. 71 (2006) 4170–4177;
(b) F.X. Felpin, E. Fouquet, A useful, reliable and safer protocol for hydrogenation and the hydrogenolysis of O-benzyl groups: the in situ preparation of an active Pd(0)/C catalyst with well-defined properties, Chemistry 16 (2010) 12440–12445;
(c) S.A. Reddy, K.C.K. Swamy, Ethanol as a hydrogenating agent: palladium-catalyzed stereoselective hydrogenation of ynamides to give enamides, Angew. Chem. Int. Ed. 56 (2017) 6984–6988.

[7] (a) A. Bhattacharjee, O.R. Seguil, J.K. De Brabander, Total synthesis and biological evaluation of apicularen A and synthetic analogs, Tetrahedron Lett. 42 (2001) 1217–1220;
(b) K. Kuramochi, Y. Osada, T. Kitahara, Synthetic study on indolic enamides, Tetrahedron 59 (2003) 9447–9454;
(c) K. Kuramochi, H. Watanabe, T. Kitahara, Synthetic Study on Oximidines: A Concise Sunthesis of (Z)-enamides, Synlett, 2000, pp. 397–399.

[8] (For selected examples, see): (a) J.M. Lee, D.-S. Ahn, D.Y. Jung, J. Lee, Y. Do, S.K. Kim, S. Chang, Hydrogen-bond-directed highly stereoselective synthesis of Z-enamides via Pd-catalyzed oxidative amidation of conjugated olefins, J. Am. Chem. Soc. 128 (2006) 12954–12962;
(b) N. Panda, A.K. Jena, M. Raghavender, Stereoselective synthesis of enamides by palladium catalyzed coupling of amides with electron deficient olefins, ACS Catal. 2 (2012) 539–543;
(c) A. Delforge, I. Georgiou, A. Kremer, J. Wouters, D. Bonifazi, Synthesis of tertiary enamides by Ag_2CO_3-promoted Pd-catalyzed alkenylation of acyclic secondary amides, Org. Lett. 18 (2016) 4844–4847;
(d) F.-X. Felpin, E. Fouquet, A useful, reliable and safer protocol for hydrogenation and the hydrogenolysis of *O*-benzyl groups: the in situ preparation of an active Pd0/C catalyst with well-defined properties, Chem. Eur J. 16 (2010) 12440–12445;
(e) K.-N.T. Tseng, J.W. Kampf, N.K. Szymczak, Modular attachment of append boron lewis acids to a ruthenium pincer catalyst: metal-ligand cooperativity enables selective alkyne hydrogenation, J. Am. Chem. Soc. 138 (2016) 10378–10381;
(f) K. Tokmic, A.R. Fout, Alkyne semihydrogenation with a well-defined nonclassical Co-H_2 catalyst: a H_2 spin on isomerization and E-selectivity, J. Am. Chem. Soc. 138 (2016) 13700–13705.

[9] S. Debbarma, S.S. Bera, M.S. Maji, Harnessing stereopecific Z-enamides through silver-free $Cp^*Rh(III)$ catalysis by using isoxazoles as masked electrophiles, Org. Lett. 21 (2019) 835–839.

[10] (For selected examples, see): (a) C. Yang, S. Gao, H. Yao, A. Lin, Rhodium-catalyzed hydroacylation of para-quinone methides with salicylaldehydes: an approach to α,α-diaryl-2-hydroxy acetopheones, J. Org. Chem. 81 (2016) 11956–11964;
(b) D. Wang, S. Cui, Rh(III)-catalyzed aldehyde C-H bond functionalization of salicylaldehydes with arylboronic acids, Tetrahedron 71 (2015) 8511–8516;
(c) A. Vijayan, T.V. Baiju, E. Jijy, P. Prakash, M. Shimi, N. Joseph, P.M. Pihko, S. Varughese, K.V. Radhakrishnan, An easy access to fused chromanones via rhodium catalyzed oxidative coupling of salicylaldehydes with heterobicyclic olefins, Tetrahedron 72 (2016) 4007–4015;
(d) K. Kokubo, K. Matsumasa, M. Miura, M. Nomura, Rhodium-catalyzed coupling reaction of salicyl aldehydes with alkynes via cleavage of the aldehyde C-H bond, J. Org. Chem. 62 (1997), 4564-4265;
(e) K. Kokubo, K. Matsumasa, Y. Nishinaka, M. Miura, M. Reaction of 2-hydroxybenzaldehydes with alkynes, alkenes, or allenes via cleavage of the aldehyde C-H bond using a rhodium catalyst system, Nomura, Bull. Chem. Soc. Jpn. 72 (1999) 303–311;
(f) J. Yang, N. Yoshikai, Cobalt-catalyzed annulation of salicylaldehydes and alkynes to form chromones and 4-chromanones, Angew. Chem. Int. Ed. 55 (2016) 2870–2874;
(g) M.L.N. Rao, B.S. Ramakrishna, Rhodium-catalyzed directing-group-assisted aldehydic C-H arylations with aryl halides, Eur. J. Org. Chem. (2017) 5080–5093.

[11] (For selected examples, see): (a) Z. Shi, N. Schröder, F. Glorius, Rhodium(III)-catalyzed dehydrogenative Heck reaction salicylaldehydes, Angew. Chem. Int. Ed. 51 (2012) 8092–8096;
(b) B. Xiao, T.-J. Gong, Z.-J. Liu, D.-F. Huo, J. Xu, L. Liu, Synthesis of dibenzofurans via palladium-catalyzed phenol-directed C-Hactivation/C-O cyclization, J. Am. Chem. Soc. 133 (2011) 9250–9253;
(c) P. Sun, S. Gao, C. Yang, S. Guo, A. Lin, H. Yao, Controllable Rh(III)-catalyzed annulation between salicylaldehydes and diazo compounds: divergent synthesis of chromones and benzofurans, Org. Lett. 18 (2016) 6464–6467;
(d) S. Debbarma, M.R. Sk, B. Modak, M.S. Maji, On-water $Cp^*Ir(III)$-catalyzed C-H functionalization for the synthesis of chromones through annulation of salicylaldehydes with diazo-ketones, J. Org. Chem. 84 (2019) 6207–6216;
(e) G.-D. Xu, Z.-Z. Huang, A Rh(III)-catalyzed cascade C-H functionalizatin/cyclization reaction of salicylaldehydes with diazomalonates for the synthesis of 4-hydroxycoumarin derivatives, New J. Chem. 42 (2018) 18358–18362;
(f) E. Jijy, P. Prakash, M. Shimi, P.M. Pihko, N. Joseph, K.V. Radhakrishnan, Rhodium catalyzed oxidative coupling of salicylaldehydes with diazabicyclic olefins: a one pot strategy involving aldehyde C-H cleavage and π-allyl chemistry towards the synthesis of fused ring chromanones, Chem. Commun. 49 (2013) 7349–7351;
(g) S. Debbarma, M.S. Maji, Cp^*Rh^{III}-catalyzed directed amidation of aldehydes with anthranils, Eur. J. Org. Chem. (2017) 3699–3706.

[12] M.J. Frisch, G.W. Trucks, H.B. Schlegel, G.E. Scuseria, M.A. Robb, J.R. Cheeseman, G. Scalmani, V. Barone, B. Mennucci, G.A. Petersson, H. Nakatsuji, M. Caricato, X. Li, H.P. Hratchian, A.F. Izmaylov, J. Bloino, G. Zheng, J.L. Sonnenberg, M. Hada, M. Ehara, K. Toyota, R. Fukuda, J. Hasegawa, M. Ishida, T. Nakajima, Y. Honda, O. Kitao, H. Nakai, T. Vreven, J.A. Montgomery Jr., J.E. Peralta, F. Ogliaro, M. Bearpark, J.J. Heyd, E. Brothers, K.N. Kudin, V.N. Staroverov, T. Keith, R. Kobayashi, J. Normand, K. Raghavachari, A. Rendell, J.C. Burant, S.S. Iyengar, J. Tomasi, M. Cossi, N. Rega, J.M. Millam, M. Klene, J.E. Knox, J.B. Cross, V. Bakken, C. Adamo, J. Jaramillo, R. Gomperts, R.E. Stratmann, O. Yazyev, A.J. Austin, R. Cammi, C. Pomelli, J.W. Ochterski, R.L. Martin, K. Morokuma, V.G. Zakrzewski, G.A. Voth, P. Salvador, J.J. Dannenberg, S. Dapprich, A.D. Daniels, O. Farkas, J.B. Foresman, J.V. Ortiz, J. Cioslowski, D.J. Fox, Gaussian 09, Revision D.01, Gaussian, Inc., Wallingford CT, 2013.

[13] (a) Y. Zhao, D.G. Truhlar, Density functionals with broad applicability in chemistry, Acc. Chem. Res. 41 (2008) 157–167;
(b) Y. Zhao, D.G. Truhlar, The M06 suite of density functionals for main group thermochemistry, thermochemical kinetics, noncovalent interactions, excited states, and transition elements: two new functionals and systematic testing of four M06-class functionals and 12 other functionals, Theor. Chem. Acc. 120 (2008) 215–241;
(c) D.G. Truhlar, Molecular modeling of complex chemical systems, J. Am. Chem. Soc. 130 (2008) 16824–16827;
(d) Y. Zhao, D.G. Truhlar, Benchmark energetic data in a model system for grubbs II metathesis catalysis and their use for the development, assessment, and validation of electronic structure methods, J. Chem. Theory Comput. 5 (2009) 324–333.

[14] (For the comments on utilizing ultrafine grid in DFT calculations): (a) J. Grafenstein, D. Izotov, D. Cremer, Dispersion interactions within the Piris natural orbital functional theory: the helium dimer, J. Chem. Phys. 127 (2007) 214103;
(b) E.R. Johnson, A.D. Becke, C.D. Sherrill, G.A. DiLabio, Oscillations in meta-generalized-gradient approximation potential energy surfaces for dispersion-bound complexes, J. Chem. Phys. 131 (2009), 034111;
(c) S.E. Wheeler, K.N. Houk, Integration grid errors for meta-GGA-predicted reaction energies: origin of grid errors for the M06 suite of functionals, J. Chem. Theory Comput. 6 (2010) 395–404;
(d) Y.-Y. Jiang, X. Man, S. Bi, Advances in theoretical study on transition-metal-catalyzed C-H activation, Sci. China Chem. 59 (2016) 1448–1466.

[15] (a) W.R. Wadt, P.J. Hay, Ab initio effective core potentials for molecular calculations. Potential for main group elements sodium to bismuth, J. Chem. Phys. 82 (1985) 284–298;
(b) P.J. Hay, W.R. Wadt, Ab initio effective core potentials for molecular calculations. Potentials for the transition metal atoms scandium to mercury, J. Chem. Phys. 82 (1985) 299–310.

[16] S. Huzinaga, Basis sets for molecular calculations, Comput. Phys. Rep. 2 (1985) 281–339.

[17] (a) K. Fukui, Formulation of the reaction coordinate, J. Phys. Chem. 74 (1970) 4161–4163;
(b) K. Fukui, The path of chemical reactions-the IRC approach, Acc. Chem. Res. 14 (1981) 363–368.

[18] (a) M. Dolg, U. Wedig, H. Stoll, H. Preuss, Energy-adjusted abinitio pseudopotentials for the first row transition elements, J. Chem. Phys. 86 (1987) 866–872;
(b) D. Andrae, U. Haussermann, M. Dolg, H. Stoll, H. Preuss, Energy-adjusted abinitio pseudopotentials for the 2nd and 3rd row transition-elements, Theor. Chem. Acc. 77 (1990) 123–141.

[19] (a) A.D. Becke, Density-functional thermochemistry. III. The role of exact exchange, J. Chem. Phys. 98 (1993) 5648–5652;
(b) C. Lee, W. Yang, R.G. Parr, Development of the colle-salvetti

correlationenergy formula into a functional of the electron density, Phys. Rev. B Condens. Matter Mater. Phys. 37 (1988) 785–789.

[20] Y. Zhao, D.G. Truhlar, A new local density functional for main-group thermochemistry, transition metal bonding, thermochemical kinetics, and noncovalent interactions, J. Chem. Phys. 125 (2006) 194101.

[21] J.-D. Chai, M. Head-Gordon, Long-range corrected hybrid density functionals with damped atom–atom dispersion corrections, Phys. Chem. Chem. Phys. 10 (2008) 6615–6620.

[22] (For selected examples for CMD C-H functionalizations): (a) X.-X. Ma, J.-B. Liu, F. Huang, C.-Z. Sun, D.-Z. Chen, O-substituted groups-controlled selectivity in Rh(III)-catalyzed coupling of benzamides with α,α-difluoromethylene alkynes: a computational mechanistic study, Catal. Sci. Tech. 8 (2018) 3590–3598;
(b) B. Ling, Y. Liu, Y.-Y. Jiang, P. Liu, S. Bi, Mechanistic insights into the ruthenium-catalyzed [4+1] annulation of benzamides and propargyl alcohols by DFT studies, Organometallics 38 (2019) 1877–1886;
(c) A.P. Walsh, W.D. Jones, Mechanistic insights of a concerted metalation-deprotonation reaction with $[Cp^*RhCl_2]_2$, Organometallics 34 (2015) 3400–3407;
(d) C. Deng, W.H. Lam, Z. Lin, Computational studies on Rhodium(III) catalyzed C-H functionalization versus deoxygenation of quinoline N-Oxides with diazo compounds, Organometallics 36 (2017) 650–656.

[23] (a) D.H. Ess, K.N. Houk, Distortion/interaction energy control of 1,3-dipolar cycloaddition reactivity, J. Am. Chem. Soc. 129 (2007) 10646–10647;
(b) Y. Yang, P. Liu, Mechanism and origins of selectivities in the copper-catalyzed dearomatization-included ortho C-H cyanation of vinylarenes, ACS Catal. 5 (2015) 2944–2951;
(c) A.K. Sharma, W.M.C. Sameera, Y. Takeda, S. Minakata, Computational study on the mechanism and origin of the regioselectivity and stereospecificity in Pd/SIPr-catalyzed ring opening cross-coupling of 2-arylaziridines with arylboronic acids, ACS Catal. 9 (2019) 4582–4592;
(d) G. Huang, Y. Xia, Catalyst-controlled C-C σ bond cleavages in metal halide-catalyzed cycloisomerization of 3-acylcyclopropenes via a formal 1,1-halometalation mechanism: insights from quantum chemical calculations, ACS Catal. 5 (2015) 859–868;
(e) X. Yang, Y. Yang, Y. Xue, Computational mechanism study of catalyst-dependent competitive 1,2-C→C, -O→C, -N→C migrations from β-methylene-β-amido-α-diazoacetate: insight into the origins of chemoselectivity, ACS Catal. 6 (2016) 162–175.

[24] (For selected examples, see): (a) W.-J. van Zeist, F.M. Bickelhaupt, The activation strain model of chemical reactivity, Org. Biomol. Chem. 8 (2010) 3118–3127;
(b) I. Fernández, F.P. Cossío, F.M. Bickelhaupt, Aromaticity and activation strain analysis of [3+2] cycloaddition reactions between group 14 heteroallenes and triple bonds, J. Org. Chem. 76 (2011) 2310–2314;
(c) I. Fernández, F.M. Bickelhaupt, Alder-ene reaction: aromaticity and activation-strain analysis, J. Comput. Chem. 33 (2012) 509–516;
(d) I. Fernández, L.P. Wolters, F.M. Bickelhaupt, Controlling the oxidative addition ofaryl halides to Au(I), J. Comput. Chem. 35 (2014) 2140–2145.

[25] (a) Y. Duan, Y. Liu, S. Bi, B. Ling, Y.-Y. Jiang, P. Liu, Theoretical study of gold-catalyzed cyclization of 2-alkynel-N-propargylanilines and rationalization of kinetic experimental pehnomena, J. Org. Chem. 81 (2016) 9381–9388;
(b) S. Kozuch, S. Shaik, How to conceptualize catalytic cycles? The energetic span model, Accounts Chem. Res. 44 (2011) 101–110.